Journal of Power Sources 195 (2010) 1316–1324

Contents lists available at ScienceDirect

Journal of Power Sources

journal homepage: www.elsevier.com/locate/jpowsour

Effect of various coal gas contaminants on the performance of solid oxide fuel cells: Part III. Synergistic effects

JianEr Bao*, Gopala N. Krishnan, Palitha Jayaweera, Angel Sanjurjo

SRI International, 333 Ravenswood Ave, Menlo Park, CA 94025, USA

ARTICLE INFO

Article history:
Received 16 June 2009
Received in revised form 9 September 2009
Accepted 9 September 2009
Available online 16 September 2009

Keywords:
Solid oxide fuel cell
Fuel contaminant
Coal syngas
Poisoning
Performance degradation
Synergistic effect

ABSTRACT

The coal-derived gas from a coal gasifier contains multiple contaminants, and their synergistic effects may not be simply the additive influences of individual contaminants. The present work presents the results of a study of the synergistic effects of four contaminants of major concern—S, As, P, and Cl, at the ppm level and in combinations of two, three, or four kinds—on the performance of Ni-YSZ/YSZ/LSM solid oxide fuel cells. The results indicate that both cell performance and morphology differ significantly in cells exposed to a single contaminant, and that cell performance is not simply the additive influence of each contaminant. Synergistic effects can be very destructive (accelerated degradation or even cell failure) when S is in the presence with As/P, but can also be beneficial (stabilization in power density variations over time or a slowed degradation rate) when Cl is present with other contaminants. Cl can even partially restore performance loss when it is introduced after P is already present. Therefore, with the addition of Cl the tolerance limit of SOFCs for the other three contaminants can be greatly increased. We speculate that the affinity of the contaminants to Ni catalyst increases in the following order: As < P < Cl. The interactions between and among these contaminants and possible mechanisms for their destructive and beneficial synergistic effects are discussed.

1. Introduction

Compared with internal combustion engines and thermal power plants (8–20% and 30–40% energy conversion efficiency, respectively), solid oxide fuel cells (SOFCs) have high, direct fuel-to-electricity conversion efficiencies of 45–60% (with a total efficiency of more than 80% when the cogenerated heat is also employed by a hybrid turbine system) [1], environmental compatibility (low NO_x production) and modularity, and fuel flexibility (i.e., the ability to use currently available fossil fuels). The U.S. Department of Energy's (DOE's) Solid Energy Conversion Alliance (SECA) program is pursuing the integration of SOFCs with coal gasifiers to produce clean energy technology. However, naturally occurring coals contain many impurities, and some of those impurities end up in the fuel gas stream even after the clean-up process, reaching the SOFC anode and causing performance degradation. Part I [2] of this series of articles discussed our accelerated testing (at a high concentration level, with a test period of about 100 h) to screen out the most potentially harmful contaminants for anode-supported Ni-YSZ/YSZ/LSM cells. In Part II [3], we calculated the thermochemical forms of these impurities in the SOFC operating environment and compared the results with those obtained using a high-temperature mass spectrometer. We also carried out extended tests at typical levels in a coal-derived gas stream and discussed the mechanisms causing the degradation. Those mechanisms can be divided into two main categories: (1) surface adsorption effects (e.g., when S and Cl block the active reaction sites for the fuel gases); SOFCs can recover from these effects after the chemicals are removed, and (2) bulk reaction effects (e.g., when As and P form secondary solid phases with the anode material); such performance losses are irreversible.

Many researchers have carried out tests on a single trace contaminant (work reported at workshops by Marina [4,5] is the exception), and some view the cumulative individual effects of various contaminants as additive [6]. However, *multiple* contaminants are present in coal syngas, and tests of *individual* contaminants and their assumed additive influence may not be representative of actual coal syngas operation. Depending on their poisoning mechanisms, various contaminants may interact with one another strongly, either competing for adsorption sites or compensating for one another, and their synergistic effects may be considerably more detrimental than simple addition. Alternatively, these contaminants may counteract/mitigate each other, greatly increasing the SOFC anode's limit of tolerance for them. It is thus necessary to establish a cumulative tolerance limit for coal contaminants. In the work reported here we investigated the synergistic effects for several combinations of contaminants with different or similar poisoning mechanisms (mainly As, P, S, and Cl) and possible interactions between and among them.

* Corresponding author. Tel.: +1 650 859 2166; fax: +1 650 859 2111.
E-mail address: valeriebao@gmail.com (J. Bao).

0378-7753/$ – see front matter © 2009 Elsevier B.V. All rights reserved.
doi:10.1016/j.jpowsour.2009.09.018

2. Experimental

All the SOFCs tested were anode-supported Ni-YSZ/YSZ/LSM cells acquired from InDec B.V., the Netherlands with the thickness of the anode layer, electrolyte layer and cathode layer being 5–10 μm, 4–6 μm, and 30–60 μm, respectively. The anode support layer (Ni-YSZ) was around 465–555 μm thick. An Ni mesh attached to the anode side by Ni paste was used as the anode current collector, and Au wires bonded to the cathode by Pt paste to increase the lateral transport efficiency were used as the cathode current collector. All the trace contaminants were introduced into the cell by passing a carrier gas (H_2) through G-Cal permeation devices from VICI Metronics at calibrated permeation rates, and the actual concentration of each contaminant was double checked using Kitagawa precision gas detector tubes from Matheson Tri-Gas (the concentration levels presented here are based on the results given by the detector tubes). The simulated coal-derived gas (syngas) mixture, which had an overall composition of 30% CO, 30.6% H_2, 11.8% CO_2, and 27.6% H_2O steam, was passed over the anode chamber at a flow rate of ~100 ml min^{-1} (STP).

Details of the cell setup, data measurement, and post experiment characterization were presented in previous papers [2,3]. All the cells were tested at a current density of 0.222 A cm^{-2} at 750 °C.

3. Results and discussion

3.1. Effects of H_2S and PH_3

The cell was first conditioned in clean syngas for 24 h or longer to establish a base line, and then the contaminants were introduced. Fig. 1 shows the synergistic effect of 1.3 ppm H_2S and 1 ppm PH_3 on the power density of the cell at 750 °C over a period of 300 h. Previously, it had been demonstrated that the presence of 1 ppm H_2S alone caused immediate performance degradation (~5 mW cm^{-2} or ~3.5%), but no appreciable long-term effects [3,7–10], whereas 0.5 ppm PH_3 formed secondary solid phases with the anode materials and caused continuous and slow degradation of ~6% in the power density over the first 300 h after which an accelerated degradation occurred [3]. Fig. 1(a) shows that after 10 days' exposure to 1.3 ppm H_2S and 1 ppm PH_3, the open circuit potential (OCV) decreased by more than 0.1 V and that the peak power density also decreased significantly. Fig. 1(b) indicates that on the introduction of 1.3 ppm H_2S and 1 ppm PH_3, the performance deteriorated immediately, followed by a steady linear degradation. Overall, the performance degraded from ~155 to ~122 mW cm^{-2} over the 315 h exposure until the cell failed (a decline of ~33 mW cm^{-2} or ~21%; the average degradation rate was ~7% every 100 h). It was also found that the cell power density declined from 150 to 140 mW cm^{-2} over a period of 400 h when 1.4 ppm PH_3 was present in the anode gas as will be manifested later in this work. Compared with that result, the presence of both S and P compounds accelerated performance degradation, and degradation occurred earlier. The cause of failure appeared to be a break in Ni current lead within the anode chamber, indicating some dramatic change induced by the synergistic effect of S and P. This finding was manifested in the morphology of the anode after exposure.

Fig. 2(a) and (b) shows the scanning electron microscope (SEM) graphs of the Ni current collector with low P level (4–15 at.% and high P level (30–40 at.%), respectively. The surface exposed to the high P level appears to be relatively rougher than that exposed to the low P level. Our previous paper [3] indicated that P could form several phosphides with Ni: Ni_3P, Ni_5P_2, and Ni_2P. The varying content of P may be indicative of the formation of a phosphide mixture. Under high magnification, the Ni wires with the high P level (Fig. 2(c)) were observed to form nanowhiskers, and the tips

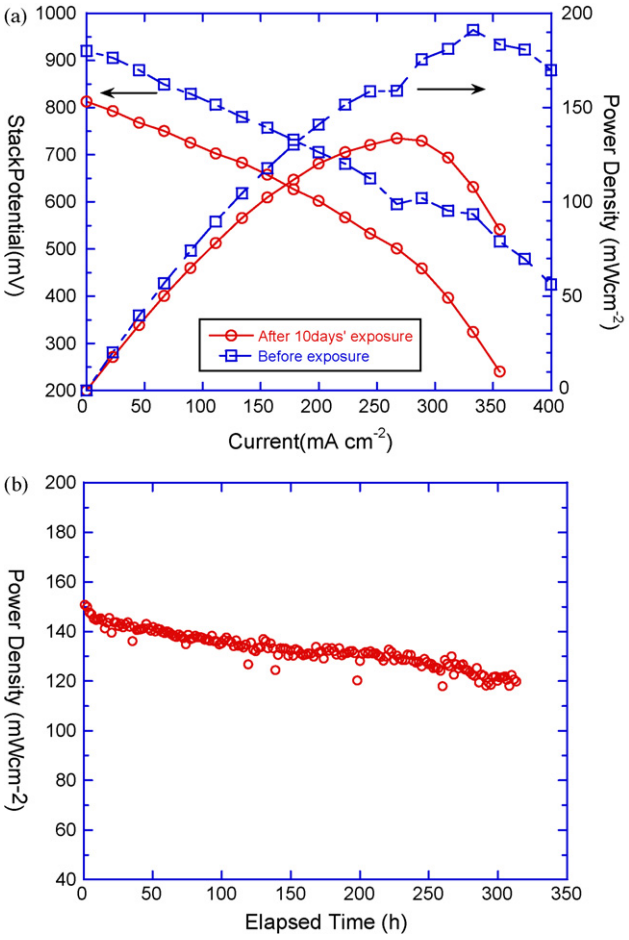

Fig. 1. Effect of 1.3 ppm H_2S and 1 ppm PH_3 on the performance of an SOFC at 750 °C. (a) *I–V* curves before and after exposure and (b) power density as a function of exposure time.

of the whiskers appeared to be rounded. Such morphology may be indicative of a liquid phase formation near the whiskers. Because of the small size of the whiskers, we were unable to measure the composition of the solidified droplet by means of energy-dispersive X-ray spectroscopy (EDX) in our SEM system. On the top of the anode surface where the porous Ni paste was found, P accumulation in the range of 5–30 at.% was also observed, depending on the area analyzed. On closer examination of the porous Ni area with high P content, nanowhiskers similar to the one described above were also observed. However, no S was detected within the resolution range of our SEM equipment, demonstrating again that no secondary phase was formed between S and the anode material and that the effect of S species is mainly dissociative adsorption of S at the catalyst surface.

According to the Ni–P phase diagram [11], compound Ni_3P melts at 950 °C and a eutectic composition of 19 at.% P–81 at.% Ni melts at 870 °C. A similar eutectic point occurs at 900 °C in the Ni–S system at 33 at.% S [11]. The formation of a liquid phase at 750 °C indicated that the melting point of the Ni–P alloy may have been lowered by the adsorption of S, because no such morphology was observed when the cell was exposed to P alone at this temperature. We were not able to find published data on the ternary Ni–S–P system, but it is not unusual that the melting point of a binary alloy is depressed when a third element is added. The observation of the nanowhiskers, indicative of liquid formation, warrants further studies of this ternary system. The formation of a liquid phase could also have resulted in the restructuring and densification of

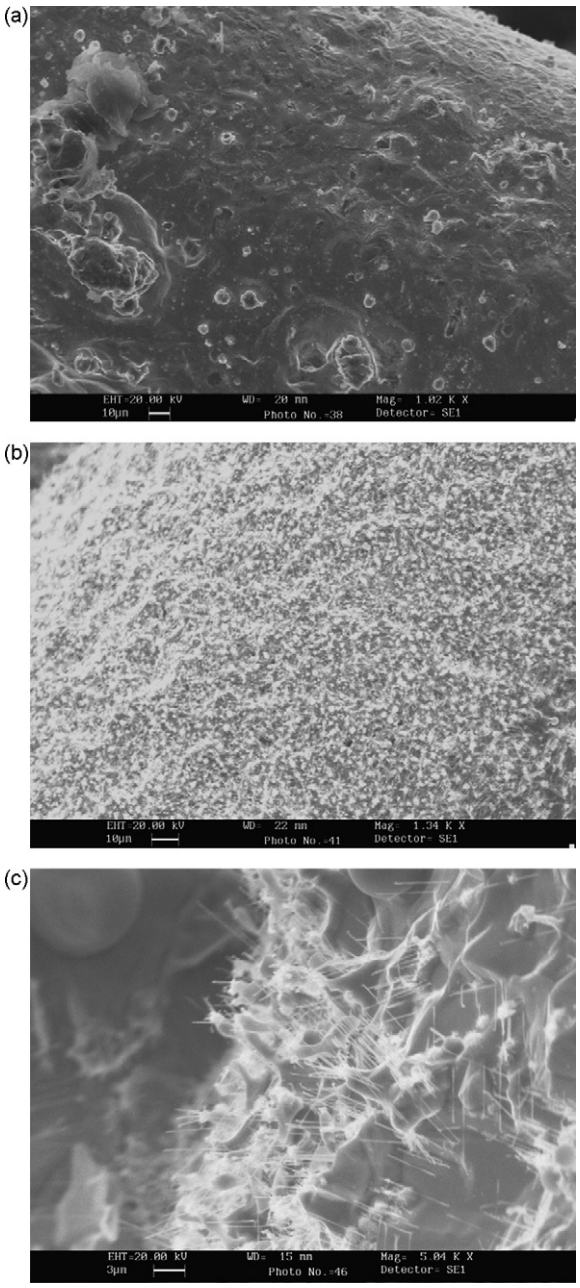

Fig. 2. Surface morphology of the anode current lead (Ni wire) after ~350 h exposure to 1.3 ppm H_2S and 1 ppm PH_3. (a) the region with low P content (~7 at.%); (b) the region with high P content (~41 at.%); and (c) a magnified SEM image of the current lead with high P content.

the anode material, and hence accelerated the degradation of cell performance. Therefore, the synergistic effect of H_2S and PH_3 at the ppm level may be more detrimental than the additive influence of individual contaminants over the long term.

Marina et al. [4] also studied the synergistic effects of 1 ppm H_2S and 2 ppm PH_3 at 800 °C. They found that initial performance lay between that of PH_3 and H_2S (in their study, 1 ppm H_2S resulted in much more performance degradation than the others within several hundred hours), but the effect of S was suppressed by the presence of P after several hundred hours. Their finding about the synergistic effect of H_2S and PH_3 was similar to ours, except that the individual effect of 1 ppm H_2S was different (which also remains controversial among the published works as discussed in part II [3]).

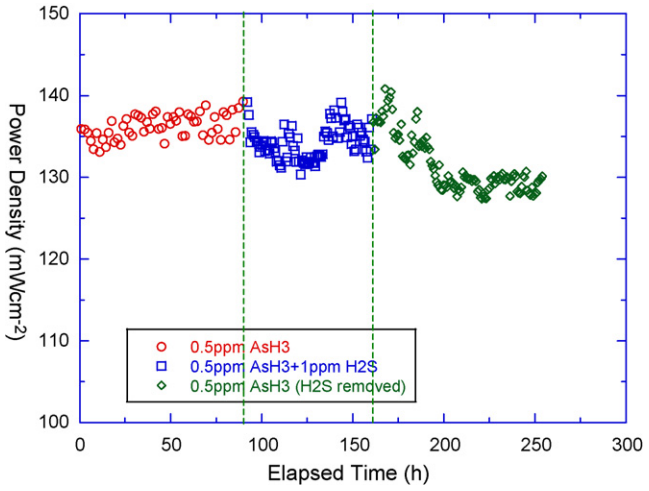

Fig. 3. Cell performance during the exposure to 0.5 ppm AsH_3 and 1 ppm H_2S at 750 °C.

3.2. Effects of H_2S and AsH_3

The effect of As is similar to that of P in that both contaminants can form a secondary solid phase with the anode material. However, the phase diagram [11] indicates that As has higher solubility in Ni (4.5 at.% at 897 °C) than does P (0.32 at.% at 870 °C); thus poisoning from As exposure generally takes place over a longer time; our previous paper [3] noted that no performance abatement occurred within 1000 h during exposure to 0.5 ppm AsH_3, but that degradation occurred after 700 h exposure to 1 ppm AsH_3; with 0.5 ppm PH_3, significant degradation occurred after 350 h exposure. Depending on the difference of the bond strength of the contaminant with the anode material, the overall synergistic effect of H_2S and AsH_3 may differ significantly from the effect of H_2S with PH_3.

Fig. 3 shows cell performance evolution during exposure to 0.5 ppm AsH_3, with the further addition of 1 ppm H_2S, and followed by the removal of 1 ppm H_2S at 750 °C. The cell was first exposed to 0.5 ppm AsH_3 alone for ~90 h, and a slight improvement in performance was seen as reported previously [3]. On the addition of 1 ppm H_2S, the performance deteriorated instantaneously, followed by partial recovery over time (~80 h), indicating that the effect of H_2S is independent of preadsorbed As species at the anode surface (in other words, presorption of As cannot mitigate the effect of H_2S). The phenomenon and the amount of initial degradation (from ~139 to 133.5 mW cm^{-2}) were similar to that observed before with 1 ppm H_2S alone. After the removal of 1 ppm H_2S, the power density initially recovered to a value even higher than indicated by previous data, but then surprisingly decreased quickly to a previous level of 140 mW cm^{-2}, followed later by a steep decrease to 129 mW cm^{-2}, remaining stable thereafter.

Significant research has been devoted to whether the effect of H_2S on SOFC performance is reversible after its removal [7,8,12–15]; and if so, whether it is instantaneously or gradually reversible and fully or partially reversible. The roles played by the test temperature (the lower the temperature, the slower the recovery rate) and the introduced concentration (full recovery at lower concentrations; e.g. 10 ppm) have also been of interest. The surprising finding in our research was that after performance recovered, it quickly decreased to a much lower level (from 136 to 129 mW cm^{-2}) before reaching a steady state. Such a significant decrease within 250 h had never been seen before with 0.5 ppm level AsH_3 alone. Whether the degradation was due to the latent synergistic effect of AsH_3 and H_2S is uncertain, but we postulate that the coadsorption of S atoms and As atoms at the anode surface caused a restructuring of the surface morphology, which may

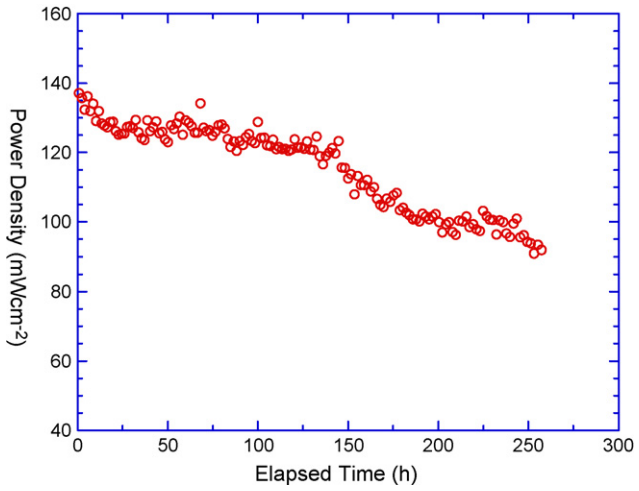

Fig. 4. Cell power density as a function of exposure time to 1.3 ppm H_2S, 1 ppm PH_3, and 0.5 ppm AsH_3 at 750 °C.

have rendered the catalyst more vulnerable to attack by As. An AC impedance spectroscopy study may provide more information regarding the cause of the performance variation. Such a study will be the subject of the next paper in this series, which will also indicate results from using other combinations of contaminants.

In a study of As poisoning of a sulfided Ni–Mo catalyst in natural gas reforming [16] using the extended X-ray absorption fine structure (EXAFS) technique, As atoms were found to be surrounded by two S atoms, and the As atoms blocked the active adsorption and reaction sites for ethane. Therefore, it can be hypothesized that As and S attack different sites at the anode and compensate for each other. Their simultaneous presence at the surface may have unexpected effects.

3.3. Effects of H_2S, PH_3, and AsH_3

Fig. 4 shows the synergistic effect of 1.3 ppm H_2S, 1 ppm PH_3, and 0.5 ppm AsH_3 on cell performance at 750 °C. From the above discussion, it could be conjectured that the synergistic effect of H_2S, PH_3, and AsH_3 is not a simple additive influence. Fig. 4 indicates that performance deteriorated immediately (from 136 to 127 mW cm^{-2}) on the introduction of contaminants, primarily as a result of 1.3 ppm H_2S addition. Following that, the power density degraded slowly for the next 100 h at a rate similar to the cell exposed to 1.3 ppm H_2S and 1 ppm PH_3, followed by accelerated degradation at the end of that period.

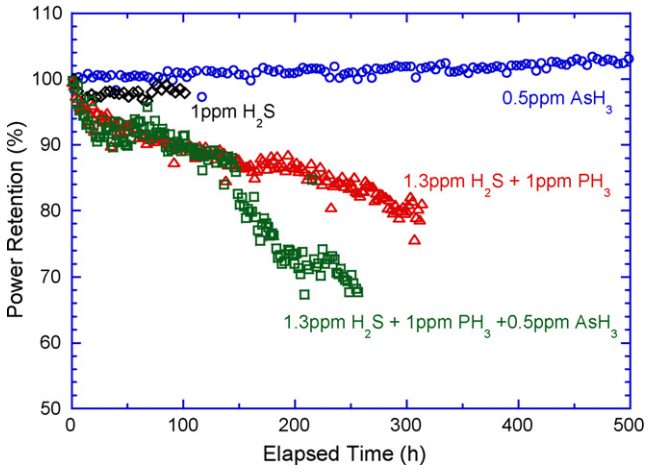

Fig. 5. Comparison of the synergistic effect of various combinations of contaminants to the cell performance in terms of the power retention with time.

Fig. 5 presents a comparison of the synergistic effect of various combinations of the contaminants. (Note the individual effect of PH_3 is not shown because the previous tested concentration was only 0.5 ppm, which may not be a good reference here, but the power retention profile of that concentration lay between those of H_2S and $H_2S + PH_3$ as can be seen from Ref. [3].) Fig. 5 clearly illustrates that:

1. AsH_3 alone, at the 0.5 ppm level, did not cause degradation over 1000 h (the data shown are not complete); however, when combined with other contaminants, AsH_3 exaggerated the detrimental effect.
2. H_2S, alone or introduced with other contaminants, caused instantaneous performance deterioration; however, when H_2S, was introduced with other contaminants, the instantaneous deterioration increased, and the more types of contaminants included, the larger the initial deterioration.
3. The power retention profile for the combination of H_2S, PH_3, and AsH_3 overlapped with that for H_2S and PH_3 for a time, but much faster degradation occurred at the end of that period for the former combination.
4. Overall, the performance deterioration under exposure to 1.3 ppm H_2S + 1 ppm PH_3 + 0.5 ppm AsH_3 was the most detrimental, exceeding the linear additive influence of individual contaminant.

These findings indicate that the synergistic effect can be very destructive when all kinds of contaminants coexisted with the coal gas as they do in realistic conditions and that the level of each contaminant may thus need to be reduced further.

3.4. Effects of CH_3Cl, AsH_3, and PH_3

A study relying on thermal desorption, low energy electron diffraction, and Auger electron spectroscopy techniques indicated the adsorption behavior of H_2 and CO on a P-adsorbed Ni surface [17], although the initial sticking coefficient and H_2 uptake were inhibited by the adsorption of P atoms on the Ni surface, that effect was significantly less when Cl or S atoms were adsorbed on the surface. Note that the study was conducted at ambient temperature, but its findings lead us to hypothesize that the affinity of Cl with Ni is probably greater than that of P with Ni. Given that the poisoning mechanism of Cl for Ni catalyst is mainly surface adsorption and that catalyst activity is recoverable after Cl removal (Trembly [18] reported the recovery of area specific resistance (ASR) after the removal of 160 ppm HCl; Richardson [19] found that the catalytic activity of Ni/Al_2O_3 for the steam reforming of methane was restored when CH_3Cl was removed.), we conjecture that Cl reduces the attack of Ni by P, mitigating the deleterious poisoning effect of P on the anode; As may have the same effect.

To study the effect of Cl-addition, we added 1 ppm CH_3Cl and 0.5 ppm AsH_3 to the anode gas of a cell that was previously exposed to 0.5 ppm AsH_3 alone for 100 h (Fig. 3). The power density was stable after the exposure to AsH_3 alone. Fig. 6 shows that a slight degradation occurred after the introduction of CH_3Cl (from 132 to 128 mW cm^{-2}), presumably due to the surface adsorption of Cl species that blocked the active catalyst sites). However, the power density then remained stable for the next 90 h. (Note that the continuous degradation during the exposure to 2.5 ppm CH_3Cl indicated in our previous study [3] may have been due to a defect in the cell and not representative of the effect of Cl.) In long-term (250 h) exposure, the power density improved slightly to ~132 mW cm^{-2}. At that point, 0.7 ppm PH_3 was introduced in the anode gas (Fig. 7). Because the power density continued to increase

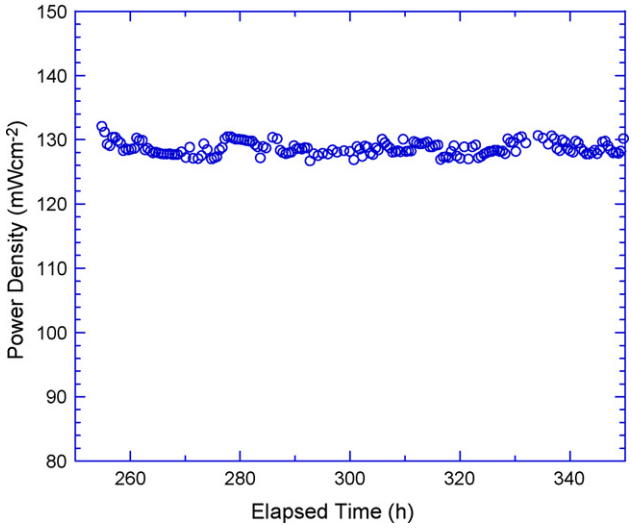

Fig. 6. Power density variation after the superimposition of 1 ppm CH_3Cl on 0.5 ppm AsH_3 at 750 °C. The cell was previously baked in 0.5 ppm AsH_3 for more than 200 h.

slowly, the amount of PH_3 in the gas was doubled to 1.4 ppm after more than 90 h. As it can be seen in Fig. 7, overall the power density remained steady for more than 340 h after the introduction of PH_3, but then started to degrade, with the data becoming very scattered, possibly due to the attack of the Ni current lead by P as observed before with PH_3 alone. The amount of CH_3Cl was then doubled as well to 2 ppm. We were surprised to note that the power density gradually stabilized again at 131 mW cm^{-2} and that data scattering was no longer observed. The experiment was terminated at this juncture because of feed gas problems.

Overall, during the 1100 h exposure to four kinds of contaminants at different concentration levels (1 ppm H_2S was removed in the middle of the experiment), only negligible power density degradation was observed. This finding is remarkable considering that the cell was exposed to PH_3 for at least 600 h and that previously we have seen that 0.5 ppm PH_3 alone caused significant degradation after 350 h at 750 °C [3]. We therefore postulate that Cl has stronger affinity with Ni and that its adsorption at the Ni surface mitigates the attack of Ni by P, thereby slowing degradation. The higher the concentration of P, the more Cl appears to be needed.

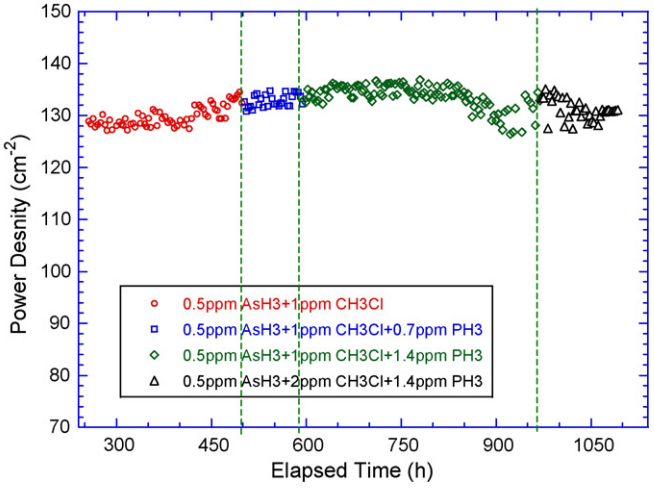

Fig. 7. Cell performance evolution during the step by step addition of 0.5 ppm AsH_3, CH_3Cl (1 ppm and 2 ppm), and PH_3 (0.7 ppm and 1.4 ppm) at 750 °C.

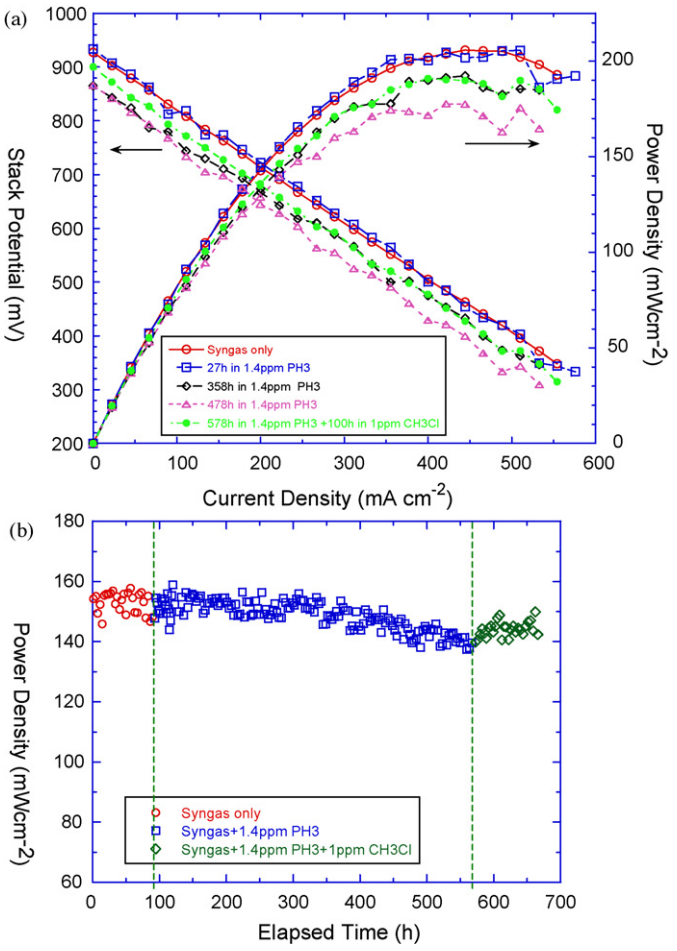

Fig. 8. Cell performance variation during exposure to 1.4 ppm PH_3 and later with the addition of 1 ppm CH_3Cl at 750 °C: (a) *I–V* profile comparison and (b) power density variation as a function of exposure time.

Another experiment further confirms the beneficial effect of Cl in inhibiting attack from P. In this case, after the cell was exposed to 1.4 ppm PH_3, slow degradation was seen after 250 h exposure as shown in Fig. 8(a) and (b) for the *I–V* profile change and the power density evolution, respectively. After more than 470 h, 1 ppm CH_3Cl was added. As Fig. 8(b) indicates, the power density quickly stopped degrading; instead, a gradual improvement was observed. Fig. 8(a) shows that after 100 h "conditioning" in 1 ppm CH_3Cl and 1.4 ppm PH_3, the OCV partly recovered (~40 mV higher than that after 358 h exposure in 1.4 ppm PH_3) and that the power densities at high current densities overlapped with those after 358 h exposure. The findings indicate that Cl, when preadsorbed on Ni catalyst surface, may not only slow or prevent much of the degradation caused by P, but when introduced after long exposure of the catalyst to PH_3, may also partly restore performance loss. Therefore, the synergistic effects of P and Cl could be quite beneficial. These findings could prove vital in designing coal gas feed systems and also in establishing tolerance limits for the anode for various contaminants. The mechanism for the recovery is still not clear, but we assume it centered on the interaction of the anode catalyst with Cl and P; conducting *in situ* surface spectrometry may determine how recovery takes place.

Fig. 9(a) and (b) shows the surface morphology of the cell anodes after exposure to 0.5 ppm AsH_3, CH_3Cl, and PH_3 (cell a), and after exposure to 1.4 ppm PH_3 and 1 ppm CH_3Cl (cell b). Fig. 9 indicates that the two cells have similar anode surface morphology, the open trench areas ("etched boundaries") are close to one another, but the

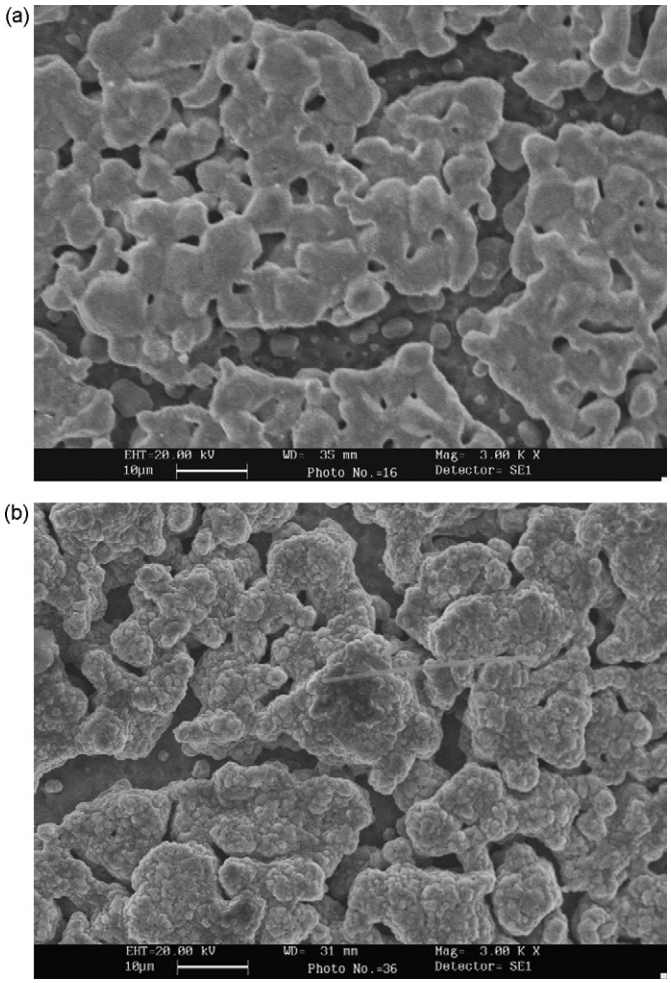

Fig. 9. SEM graphs of the cell anode after exposure: (a) cell exposed to 0.5 ppm AsH_3, CH_3Cl, and PH_3 (cell a) and (b) cell exposed to 1.4 ppm PH_3, and later with the addition of 1 ppm CH_3Cl (cell b).

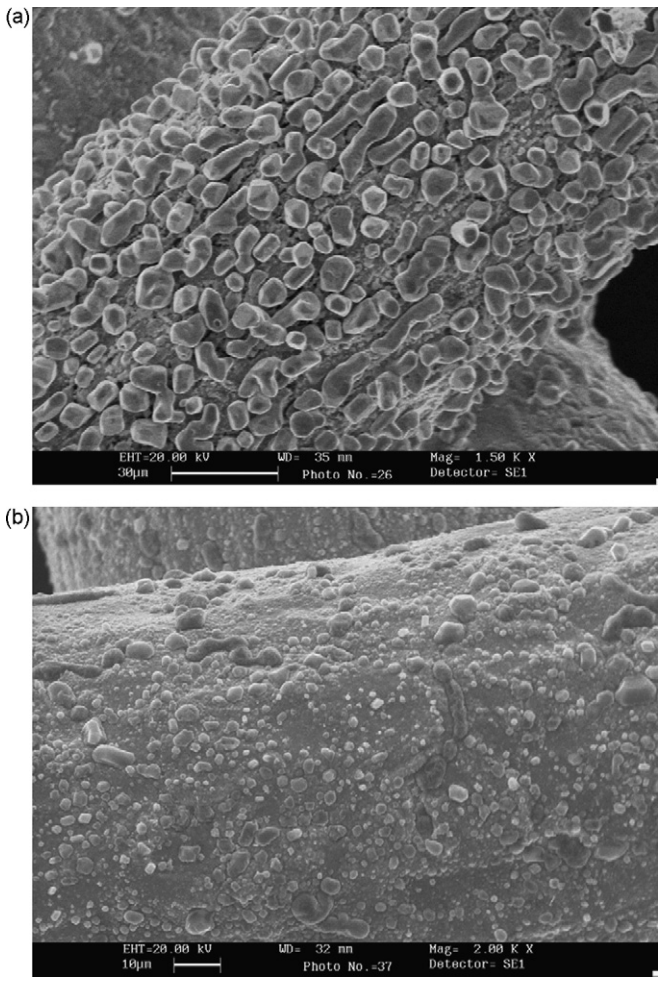

Fig. 11. SEM graphs of the Ni current lead after exposure: (a) exposed to 0.5 ppm AsH_3, CH_3Cl, and PH_3 (wire a) and (b) exposed to 1.4 ppm PH_3, and later with the addition of 1 ppm CH_3Cl (wire b).

Ni patches of the first cell seem to be slightly more densified and smoother, whereas the Ni surface of the second cell has more fine features and is rough. Such a rough catalyst surface, which has not been seen before with other kind of contaminants, may be due to the synergistic effect of P and Cl. That effect may have contributed to the partial restoration of power density after the superimposition of CH_3Cl on PH_3, given that the active catalyst surface area is higher when the surface is rougher. EDX analysis of several spots on the patches for both cells showed pure Ni (some O was also detected on the rough surface of cell b, possibly absorbed during the cooling process or in the open area), and the open trenches were also rich in Ni, with varying amounts of Zr (4–35 at.%) in some trenches. Several abnormal regions are also seen at the anode surface for cell a, as shown in Fig. 10. The surface morphology is significantly different from the surrounding area; fine particles are scattered in the white contrast region, and the P level is 20–30 at.%, with the remaining element being O. It seems that P attacked weak regions and accumulated there, which may have caused the performance loss during the exposure. No As was detected within the detection limit for either cell.

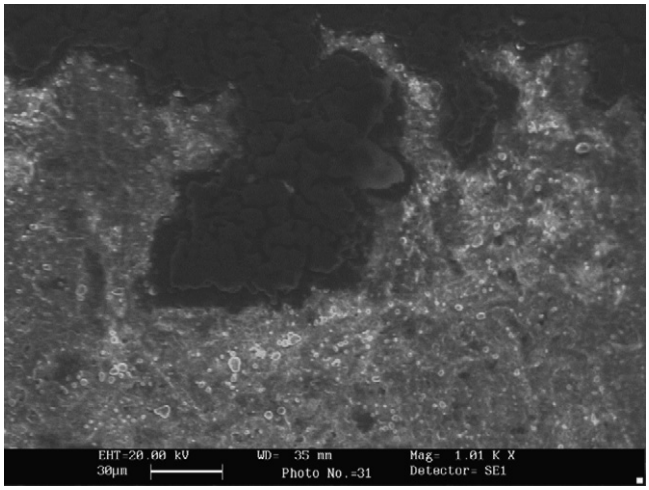

Fig. 10. An abnormal region on the anode surface.

Fig. 11 compares the surface morphology of the Ni current leads for the two cells discussed above. For wire exposed to 0.5 ppm AsH_3, CH_3Cl, and PH_3 (Fig. 11(a), wire a), numerous irregularly shaped "pebbles" are seen on top of the wire, and the surface underneath is also very rough. These pebbles are less than 10 μm in diameter and aligned along the wire direction; EDX spot analysis did not detect As or P. Pebbles were also seen at the anode surface when the cell was exposed to 35 ppm AsH_3 in an accelerated test [2]; in that case, however, a high level of As in the anode was detected with EDX. We postulate that the As/P engraved the Ni wire surface at the beginning, but that the excess amount of Cl subse-

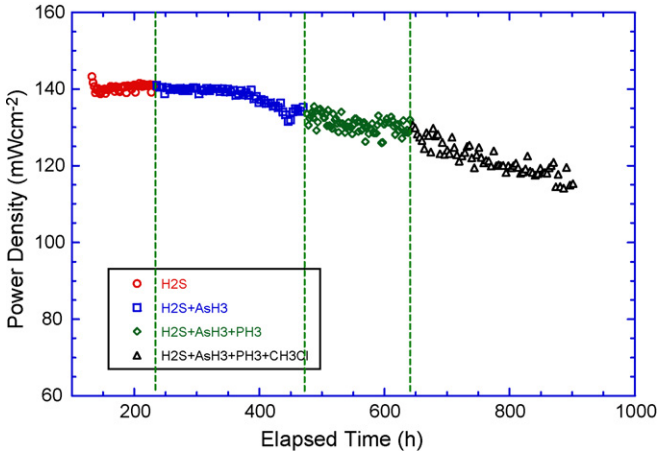

Fig. 12. Cell performance variation during the exposure to 1 ppm H_2S, 0.5 ppm AsH_3, 0.5 ppm PH_3, and 1 ppm CH_3Cl in sequential addition at 750 °C.

quently replaced the As/P species at the surface. In Fig. 11(b), much smaller pebbles are seen at the wire surface for cell b, most seem to have just nucleated, and the remaining surface still looks smooth. EDX spot analysis showed that on the smooth surface area, only 0.55–6.95 at.% of P was detected, but on the pebbles, a relatively high level of P (~10 at.%) was detected. The first cell was exposed to 0.5 ppm AsH_3 for ~1100 h, 0.7 to 1.4 ppm PH_3 for 600 h, and to 1 ppm CH_3Cl for more than 800 h (raised to 2 ppm during the last 150 h); the second cell was exposed to 1.4 ppm PH_3 for ~600 h, but exposed to 1 ppm CH_3Cl for only ~100 h. It is thus understandable that the current lead for the first cell has a clearly carved surface, given it was etched for a longer time. We surmise that Cl would have further replaced As/P if the experiment for cell b had continued. From these results, we speculate that the affinity of these contaminants increases in this order: As < P < Cl.

P was also detected in the bulk of the anode support layer for both cells, with the amount varying from ~2 to 12 at.%, but no As was detected. A higher level of Cl or longer exposure in Cl may be needed to replace the P.

3.5. *Effects of H_2S, AsH_3, PH_3, and CH_3Cl*

For the first cell (cell a) discussed in Section 3.4 in regard to interactions among Cl, As, and P, 1 ppm H_2S was removed before the introduction of Cl and P; therefore, the synergistic effect of S with other contaminants could not be determined. In the experiment discussed here, all four contaminants of major concern were included, but introduced sequentially (additively), not simultaneously.

Fig. 12 shows the power density evolution during the series exposure to 1 ppm H_2S, 0.5 ppm AsH_3, 0.5 ppm PH_3, and 1 ppm CH_3Cl. The trace-level contaminants were introduced in this manner because the presence of H_2S alone causes a certain level of initial degradation but not long standing degradation, but the presence of AsH_3 and PH_3 causes a slow and rapid decrease in the power density, respectively. The presence of CH_3Cl appears to retard the effect of other contaminants.

After the introduction of 1 ppm H_2S, the power density decreased instantaneously from 143.5 to 138.5 mW cm^{-2}, but then slowly improved to 141 mW cm^{-2} over the ~100 h of exposure. After that, 0.5 ppm AsH_3 was introduced in addition to H_2S. No degradation was seen within the first 120 h; after that point, the power density declined slowly. However, the power density seemed to stabilize for 20 h after that period. Unlike that for Cl, S preadsorption at the catalyst surface did not prevent/mitigate As attack on the catalyst; instead, it accelerated degradation. We

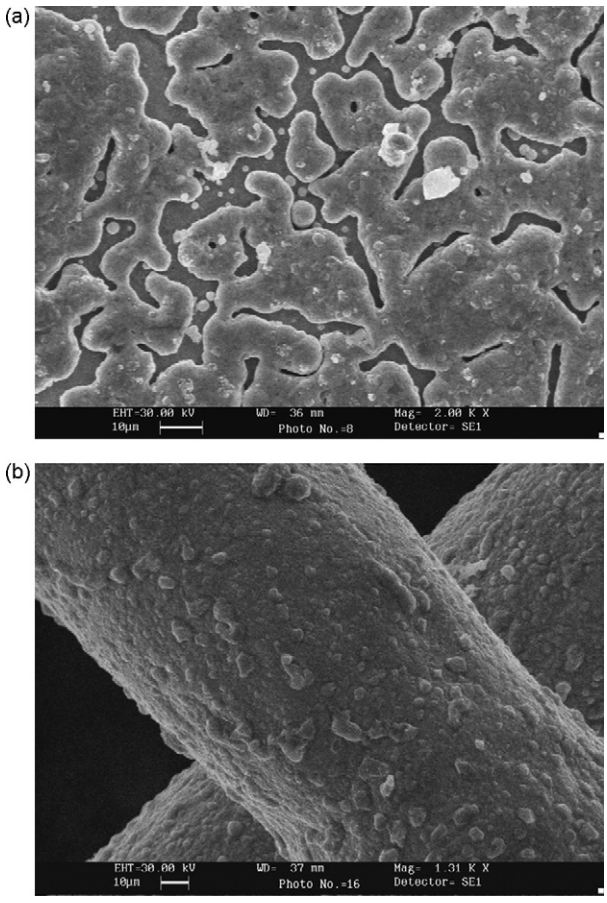

Fig. 13. SEM graphs of the (a) cell anode top surface and (b) Ni current lead after series exposure to four contaminants.

speculate that S and As attack different sites of the catalyst, not only blocking the active adsorption and reaction regions (the three-phase boundaries) for the fuel gas, but also form a secondary solid phase with the catalyst. After more than 240 h in H_2S and AsH_3, 0.5 ppm PH_3 was introduced. Degradation continued slowly, but once more, performance seemed to stabilize after 100 h. After around 200 h exposure in these three contaminants, 1 ppm CH_3Cl was introduced. The power density continue to degrade contrary to our previous finding that Cl mitigated the deleterious effect of As and P. Overall, the cell power density decreased from ~143.5 to ~117 mW cm^{-2} over the 775 h exposure; that decline was less severe than that resulting from exposure to 0.5 ppm PH_3 alone as has been studied previously [3], considering that the cell was exposed to 0.5 ppm PH_3 for at least 475 h in addition to the other contaminants. Therefore, despite the continuous degradation during the series exposure to these four contaminants, some constructive force may still have been at work.

After the experiment, the cell morphology was characterized with SEM. Fig. 13(a) and (b) shows the morphology of the anode's top surface and the Ni current lead after exposure, respectively. Compared with the surface morphology of the two cells discussed in Section 3.4, the cell exposed to four contaminants in series is more sintered with slightly more open trenches, and the interconnectivity between each Ni patch is also broken to a greater extent. Because the cell was not exposed to contaminants for a longer time than previous cell a, we speculate that the sintering was resulted from the synergistic effects of S and As/P. Section 3.1 indicates that the addition of S may lower the melting point of the phosphide. The P level at 3–5 at.% was detected in some of the trenches and

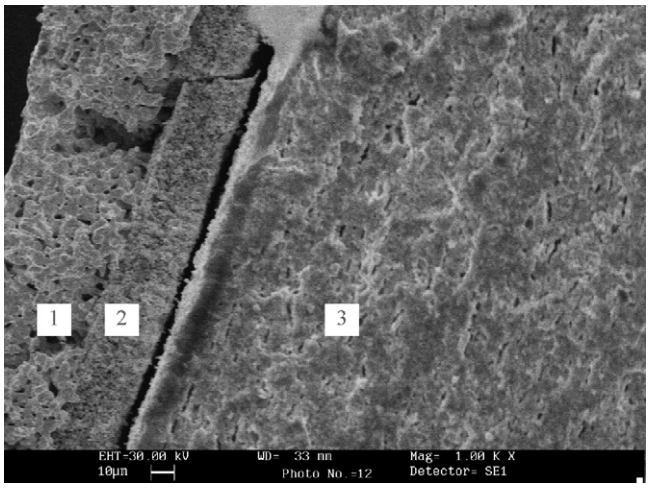

Fig. 14. SEM graph of the cell cross-section after series exposure to four contaminants.

also at the edge of a few particles in the trenches, but not on top of the large Ni patches. Because Cl was introduced only at the end of the experiment for around 255 h, it is likely that Cl could not fully replace P. However, some degree of surface roughing is also seen on the Ni patches, similar to the second cell discussed in Section 3.4; that roughing may have been caused by the replacement of P by Cl. The morphology of the Ni wire is also similar to that of the second cell discussed in Section 3.4, although with slightly fewer lumps at the surface because the exposure level of PH_3 in this case was only 0.5 ppm. However, the amount of P detected on those lumps was significantly higher than that detected for other cells. P at around the 40 at.% level was detected, presumably forming Ni phosphides, but no P was detected at the smooth surface area. This suggests that if crystal Ni phosphides are formed, Cl could not replace P, but if P only dissolves in Ni or adsorbs at the surface, Cl may replace P.

Fig. 14 shows the cross-section of the cell after exposure. Three distinctive layers are seen, from the left to right (labeled as 1, 2, and 3): the porous LSM cathode layer, the dense YSZ electrolyte layer, and the porous Ni-YSZ anode layer (including the anode support layer). Interestingly, the electrolyte layer is detached from the anode layer, and a crack is seen at the electrolyte. Although the crack may have been introduced when the cell was broken for characterization, the cell is supposed to be very strong mechanically, with each layer being tightly bonded, and such detachment of two layers has never been seen before. The anode side near the electrolyte layer also seems to have densified. Fig. 15 shows the elemental mapping of the cross-section. The figure on the top left is the secondary electron micrograph, and the others map the distribution of Ni, Zr, and P. As can be seen, Ni exists only in the anode region, with Zr distributed between the anode and electrolyte. A trace amount of P is also detected in the anode bulk, but interestingly, a relatively high density of P signals are seen at the border of the anode layer and the electrolyte layer, with no P in the electrolyte layer (a trace amount of P also seems to be detected in the cathode layer). Again, we note that because the P Kα peak (2.014 keV) is very similar to the Zr $L\alpha 1$ (2.042 keV) peak, distinguishing between the X-ray emission peaks of P and Zr at that energy range may not be accurate. However, the accumulation of P near the electrolyte may indicate the reason for the detachment of the electrolyte layer from the anode. The exact reason for the accumulation of P there is not clear, and the detachment may have partly resulted from defects in the original cell. Therefore, this accumulation may have contributed to the continuous degradation of the cell power density, and the interaction between S and other contaminants needs to be further studied. Signals for other contaminants (e.g., S, Cl, As) were difficult to distinguish from the background noise and are therefore not shown here.

4. Conclusions

The present work has studied the synergistic effects of four contaminants of major concern—As, P, S, and Cl, in combinations

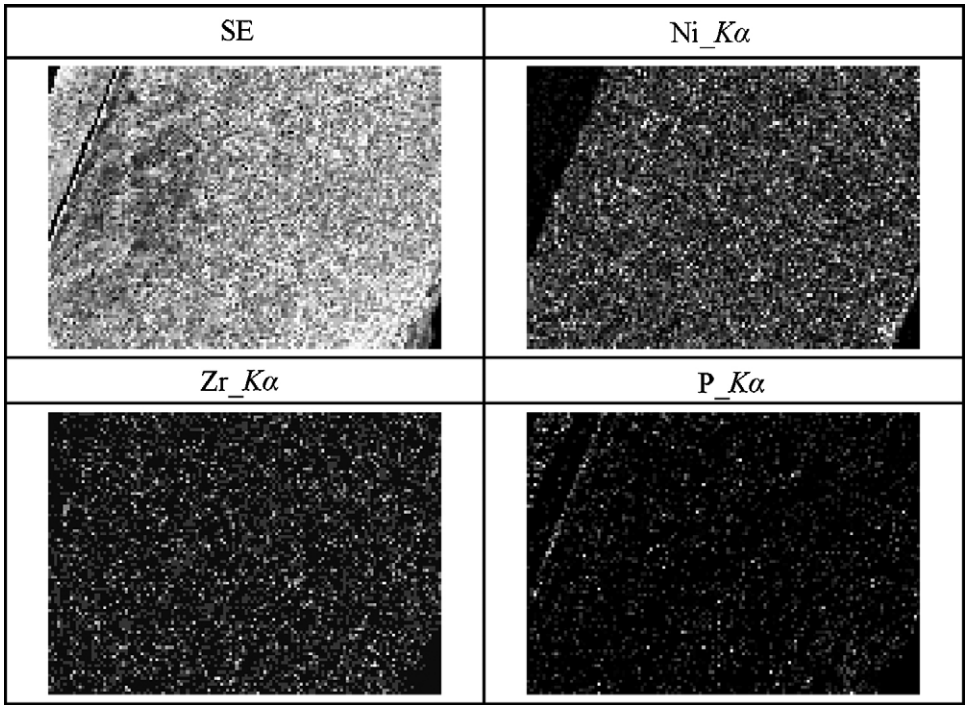

Fig. 15. Elemental mapping of the cell cross-section after series exposure to four contaminants.

of two, three, and four—on the performance of Ni-YSZ/YSZ/LSM SOFCs. Those synergistic effects are significantly different from the ones produced by individual contaminants, and are not simply the additive influence of individual contaminants. A synergistic effect can be quite destructive (e.g., accelerated cell degradation or even failure caused by the combination of 1.3 ppm H_2S + 1 ppm PH_3, 1 ppm H_2S + 0.5 ppm AsH_3, and 1.3 ppm H_2S + 1 ppm PH_3 + 0.5 ppm AsH_3) but can also be beneficial when Cl is present (e.g., combinations of 0.5 ppm AsH_3 + 1 ppm CH_3Cl [later 2 ppm] + 1.4 ppm PH_3, 1.4 ppm PH_3 + 1 ppm CH_3Cl, and 1 ppm H_2S + 0.5 ppm AsH_3 + 0.5 ppm PH_3 + 1 ppm CH_3Cl). The presence of S may lower the melting point of phosphides (and possibly arsenides) and cause the sintering/densification of the Ni catalyst. Some whiskers were also observed at the anode after exposure to H_2S and PH_3, presumably because of the formation of a liquid phase. However, the presence of Cl may have mitigated/prevented attack on the catalyst by other contaminants: power density either attained a steady state, or the degradation rate slowed over extended exposure time, depending on the amount of Cl present (currently the highest Cl level tested has been 2 ppm). We speculate that the affinity of the contaminants with the Ni catalyst increases in this order: As < P < Cl. Therefore, Cl may not only abate attacks on Ni by other contaminants when preadsorbed, but could also partially replace other contaminants when introduced later. Such replacement may cause the roughing of the catalyst surface and restore part of the performance loss. According to the results obtained in this study, the tolerance limit of SOFCs to these four major contaminants could remain at the ppm level without appreciable degradation for more than 1000 h.

Acknowledgements

The authors would like to thank DOE for its financial support under Contract DE-FC26-05NT42627. We also thank Jordi Perez-Mariano for his help with the SEM graphs.

References

[1] S.C. Singhal, MRS Bull. 25 (2000) 16–21.
[2] J. Bao, G.N. Krishnan, P. Jayaweera, J. Perez-Mariano, A. Sanjurjo, J. Power Sources 193 (2) (2009) 606–617.
[3] J. Bao, G.N. Krishnan, P. Jayaweera, K.-H. Lau, A. Sanjurjo, J. Power Sources 193 (2) (2009) 617–624.
[4] O.A. Marina, L.R. Pederson, D.J. Edwards, C.W. Coyle, J. Templeton, M. Engelhard, Z. Zhu, SOFC Operation on Hydrogen and Coal Gas in the Presence of Phosphorous, Arsenic and Sulfur Impurities, 8th Annual SECA Workshop, San Antonio, TX, 2007.
[5] O.A. Marina, L.R. Pederson, C.A. Coyle, E.C. Thomsen, D.J. Edwards, C.D. Nguyen, G.W. Coffey, Interactions of Ni/YSZ Anodes with Coal Gas Contaminants, 9th Annual SECA Workshop, Pittsburgh, PA, 2008.
[6] EG&G Technical Services, Parsons, Inc., Science Applications International Corporation, Fuel Cell Handbook, Fifth edition, Report to U.S. DOE under contract DE-AM26-99FT40575 (2004).
[7] W. Feduska, A.O. Isenberg, J. Power Sources 10 (1983) 89–102.
[8] S.C. Singhal, R.J. Ruka, J.E. Bauerle, C.J. Spengler, Anode Development for Solid Oxide Fuel Cells, Report No. DOE/MC/22046-2371 (1986).
[9] E. Batawi, U. Weissen, A. Shuler, M. Keller, C. Voisard, The Electrochemical Society Proceedings Series, vol 2001-16, edited by H. Yokokawa and S. C. Singhal, p 140-147. The Electrochemical Society Meetings, Pennington, NJ, 2001.
[10] J. Iritani, K. Kougami, N. Komiyama, K. Nagata, K. Ikeda, K. Tomida, The Electrochemical Society Proceedings Series, vol 2001-16, edited by H. Yokokawa and S. C. Singhal, p 63-71. The Electrochemical Society Meetings, Pennington, NJ, 2001.
[11] ASM International, ASM Handbook, vol. 3: Alloy Phase Diagram, 1992.
[12] S. Primdahl, M. Mogensen, Proceedings of the 5th International Symposium on Solid Oxide Fuel Cells The Electrochemical Society Proceedings Series, 99-19, 1999, pp. 530–540.
[13] Y. Matsuzaki, I. Yasuda, Solid State Ionics 132 (2000) 261–269.
[14] K. Sasaki, K. Susuki, A. Iyoshi, M. Uchimura, N. Imamura, H. Kusaba, Y. Teraoka, H. Fuchino, K. Tsujimoto, Y. Uchida, N. Jingo, Proceedings of 9th International Symposium on Solid Oxide Fuel Cells The Electrochemical Society Proceedings Series, 2005-07, 2005, pp. 1267–1274.
[15] K. Haga, S. Adachi, Y. Shiratori, K. Itoh, K. Sasaki, Solid State Ionics 179 (2008) 1427–1431.
[16] A.P. Molina, L.P. Nielsen, A.M. Molenbrook, Catal. Lett. 92 (2004) 29–34.
[17] M. Kishinova, D.W. Goodman, Surf. Sci. 108 (1981) 64–76.
[18] J.P. Trembly, R. Gemmen, D.J. Bayless, Proceedings of the 5th International Fuel Cell Science Engineering and Technology Conference, vol. 171, 2007, pp. 818–825.
[19] J.T. Richardson, J.D. Ortego, N. Coute, M.V. Twigg, Catal. Lett. 41 (1996) 17–20.